1-2-2024

A prediction of interfacial tension by using molecular dynamics simulation: A study on effects of cushion gas (CO2, N2 and CH4) for underground hydrogen storage

Quoc T. Doan
Edith Cowan University

Alireza Keshavarz
Edith Cowan University

Caetano R. Miranda

Peter Behrenbruch

Stefan Iglauer
Edith Cowan University

10.1016/j.ijhydene.2023.10.156
Doan, Q. T., Keshavarz, A., Miranda, C. R., Behrenbruch, P., & Iglauer, S. (2024). A prediction of interfacial tension by using molecular dynamics simulation: A study on effects of cushion gas (CO2, N2 and CH4) for underground hydrogen storage. International Journal of Hydrogen Energy, 50(Part D), 1607-1615. https://doi.org/10.1016/j.ijhydene.2023.10.156

International Journal of Hydrogen Energy 50 (2024) 1607–1615

Contents lists available at ScienceDirect

International Journal of Hydrogen Energy

journal homepage: www.elsevier.com/locate/he

A prediction of interfacial tension by using molecular dynamics simulation: A study on effects of cushion gas (CO_2, N_2 and CH_4) for Underground Hydrogen Storage

Quoc Truc Doan [a,c,*], Alireza Keshavarz [a], Caetano R. Miranda [b], Peter Behrenbruch [c], Stefan Iglauer [a]

[a] Centre for Sustainable Energy and Resources, Edith Cowan University, 270 Joondalup Drive, Joondalup, WA 6027 Western Australia, Australia
[b] Departamento de Física dos Materiais e Mecânica, Instituto de Física, Universidade de São Paulo, São Paulo, 05508-090 São Paulo, Brazil
[c] Bear and Brook Consulting, 135 Hilda Street, Corinda (Brisbane), 4075 Queensland, Australia

ARTICLE INFO

Keywords:
Underground Hydrogen Storage (UHS)
Carbon Capture and Storage (CCS)
Molecular dynamics simulation
Interfacial tension
Cushion gas
Depleted hydrocarbon reservoirs

ABSTRACT

Carbon Dioxide (CO_2) emissions from fossil fuel consumption have caused global warming and remain challenging problems for mitigation. Underground Hydrogen Storage (UHS) provides clean fuel and replaces traditional fossil fuels to reduce emissions of CO_2. Geological formations such as depleted oil/gas reservoirs, deep saline aquifers and shale formations have been recognized as potential targets to inject and store H_2 into the subsurface formations for large-scale implementation of CCS and UHS. However, the presence of H_2 with cushion gas at different fractions under different geo-storage conditions, which can influence Hydrogen's flow properties, was not investigated widely. Until now, studies of interfacial properties between water and a mixture of cushion gas (CO_2, N_2 or CH_4) in the presence of H_2 are very limited or unavailable data in experiments and simulations. In this study, many predictions by using molecular dynamics simulation were conducted to predict the interfacial tension (γ) for the systems of $H_2/CO_2/H_2O$, $H_2/N_2/H_2O$ and $H_2/CH_4/H_2O$ at different pressures, temperatures, and fractions of cushion gases A comparison between the predicted γ results from the simulation and previous research were also made. The findings of this study indicated that γ of $H_2/CO_2/H_2O$, $H_2/CH_4/H_2O$, and $H_2/N_2/H_2O$, as a function of pressure, temperature, and fraction of H_2, decreased with increasing pressures and temperatures and increased with increasing H_2% in the mixture. Additionally, an extending or new γ data in simulation for the $CO_2/H_2/H_2O$, $N_2/H_2/H_2O$ and $CH_4/H_2/H_2O$ systems from this study were reported and support evaluating the stability and storage capacity of H_2 combined with the cushion gas in geological formations. Furthermore, it can contribute to de-risking and proceeding safely and efficiently for the large-scale implementation of Underground Hydrogen Storage.

1. Introduction

Global warming due to Carbon Dioxide (CO_2) emissions from consuming fossil fuels remains a complicated challenge in reaching the Paris Agreement's goals [1]. Several technological solutions are offered for this problem, including Carbon Capture and Storage (CCS) and Underground Hydrogen Storage (UHS) [2,3]. The CCS solution reduces CO_2 emissions from fossil fuel power plants and carbon-intensive industries [4,5]. To cut carbon dioxide emissions, the solution of UHS supplies clean fuel and replaces conventional fossil products [6,7]. Geological formations such as depleted oil/gas reservoirs, deep saline aquifers and shale formations have been recognized as potential targets to inject and store H_2 into the subsurface formations for large-scale implementation of CCS and UHS by storage capacity and geological stability [8–10]. Specifically, in the porous media, the injected H_2 will replace the in-situ pore fluids (water or residual hydrocarbon) at the subsurface formations and be distributed under an impermeable layer or cap rock by a lower density of Hydrogen [8]. Currently, the UHS in depleted hydrocarbon reservoirs has assessed the best selection for large-scale implementation for significant reasons. First of all, geological structures and reservoir characterization data were gathered and analyzed carefully in the exploration and operation phases. Next, surface and subsurface

* Corresponding author.
E-mail address: t.doan@ecu.edu.au (Q.T. Doan).

https://doi.org/10.1016/j.ijhydene.2023.10.156
Received 28 August 2023; Received in revised form 11 October 2023; Accepted 14 October 2023
Available online 31 October 2023

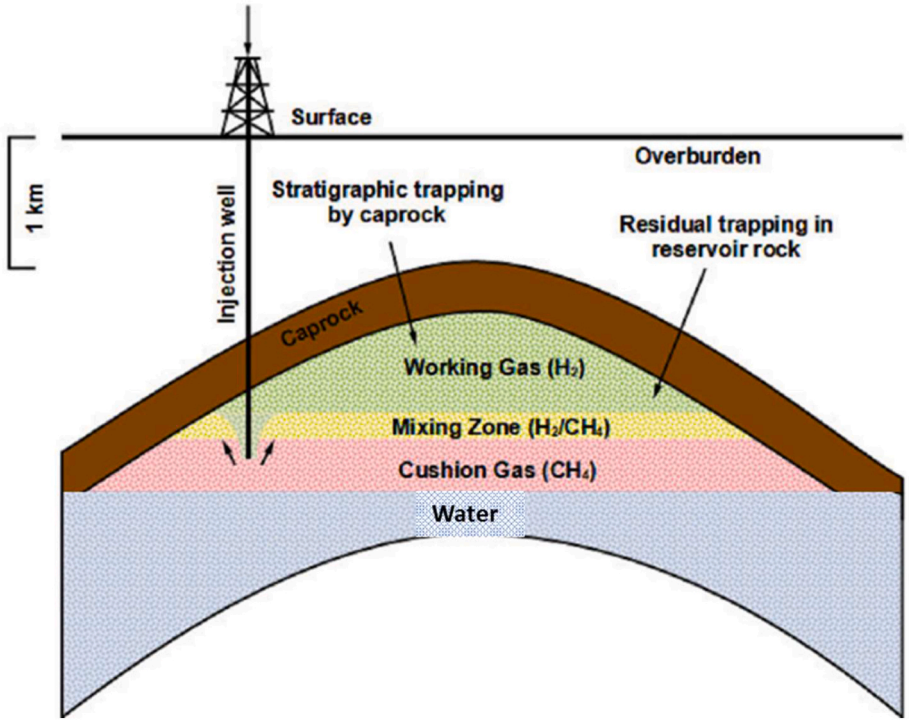

Fig. 1. A conceptual model of Underground Hydrogen Storage in depleted hydrocarbon reservoirs between Hydrogen and cushion gas (CH_4) [16].

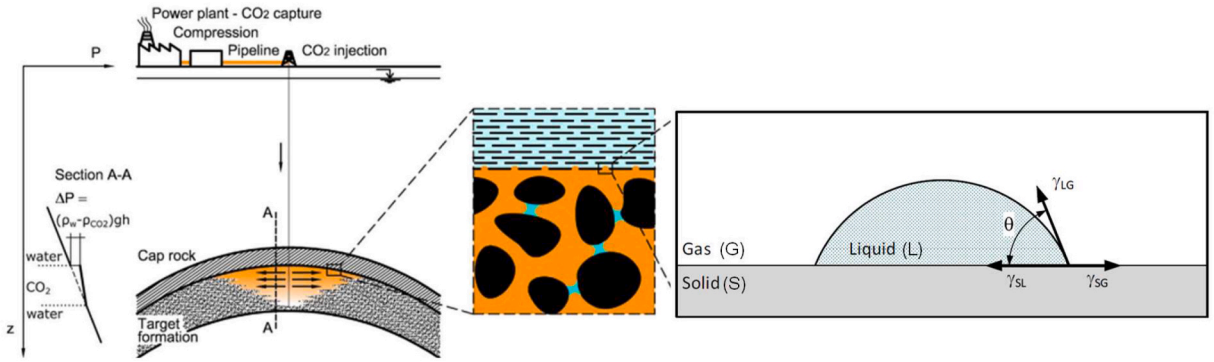

Fig. 2. A simple description of interfacial properties that influence CCS and UHS projects' reliability and storage capacity [11,24,25].

equipment of H_2 storage projects can be inherited from depleted oil/gas projects with minimal or without modification. Furthermore, many best practices and lessons learnt from gas injection for enhancing hydrocarbon recovery in the oil and gas industry are still valid and applicable to the UHS projects [11,12].

The UHS is considered in common concepts with Underground Gas Storage (UGS) [13]. In practice, a storage process at underground formations requires a cushion gas (CO_2, N_2 or CH_4) to maintain high sufficient pressure in reservoirs as working gas (or H_2) is being withdrawn and also prevent water production [10,14,15], as shown in Fig. 1. Specifically, the process requires the cushion gas to be injected into the subsurface formation before implementing the H_2 injection. It leads to forming a mixing zone that includes cushion gas and H_2 during injection [12,16]. However, the level of blending of the cushion gas and injected H_2, interactions between the gas and liquid and influences of hydrodynamics at underground formations are unclear for the UHS [12]. To date, there has been minimal study on the effects of cushion gas for implementing Hydrogen underground storage. Hence, the presence of H_2 and different fractions of cushion gas under different geo-storage conditions [8] can influence the flow characteristics of H_2 via the injection and production cycle conditions [17], which needs attention for investigation.

Accurate storage capacity assessment requires estimating the volume of H_2 that can be safely stored in subsurface formations is complicated. Because injected gas in the subsurface formations possibly escapes via caprock when the breakthrough pressure of injected gas is higher than the capillary entry pressure. So, the reliability and storage capacity for a subsurface formation is controlled significantly by capillary pressure [18–21], which is described as a function of contact angles and interfacial tensions and pore radius, as described by the equation of Young-Laplace (1)

$$P_c = P_g - P_w = \frac{2\gamma\cos\theta}{r} \quad (1)$$

where P_c is the capillary entry pressure, P_g and P_w are the pressure of the gas and water phase; γ is the interfacial tension between water and gas, θ is contact angle, and r is effective radius of the pore, as displayed in Fig. 2. The equation (1) shows that γ is a critical parameter revealing an amount of Hydrogen can be injected for storage and how the gas plume spreads in the underground formations [22,23]. Besides, the estimation

Table 1
A summary of previous studies for interfacial tension between H_2O and gas mixture in the presence of H_2.

Authors	Year	Method	Systems	Pressure, MPa	Temperature, K	Cushion Gas %
Hosseini et al.	2022	Experiment	H_2/Brine[a]	1–35	298–423	
Chow et al.	2018	Experiment	H_2/H_2O	0.5–45	298–448	
Massoudi et al.	1974	Experiment	H_2/H_2O	7.6	298.15	
Yang et al.	2022	Simulation	H_2/H_2O	1–160	298–523	
Doan et al.	2023	Simulation	H_2/H_2O	1–70	298–323	
Georgiadis et al.	2010	Experiment	CO_2/H_2O	1–60	298–374	
Kvamme et al.	2007	Experiment	CO_2/H_2O	0.1–20	278–335	
Silvestri et al.	2019	Simulation	CO_2/H_2O	1–50	308, 323 and 383	
Yan et al.	2001	Experiment	$CO_2/N_2/H_2O$	1–30	298–373	
Chow et al.	2016	Experiment	$CO_2/N_2/H_2O$	2–40	298–448	
Ren et al.	2000	Experiment	CH_4/H_2O	1–30	298–373	
Naeiji et al.	2020	Simulation	CH_4/H_2O	1.4–10	275–323	
Chow et al.	2018	Experiment	H_2–CO_2-Water	0.5–45	298 to 448	CO_2 (30 %)
Isfehani et al.	2023	Experiment	H_2–CO_2-Water	3–20	323	CO_2 (30%–70 %)
Mirchi et al.	2022	Experiment	H_2–CH_4-Brine[a]	6.9	295, 313 and 333	CH_4 (20%–80 %)
Alanazi et al.	2023	Experiment	H_2–CH_4-Brine[a]	0–11	323	CH_4 (50 %)
Doan et al.	2023	Simulation	H_2–CH_4-Water	1.0–70	300	CH_4 (40 %)

[a] Brine is from NaCl.

of the interfacial tensions of H_2 in the presence of subsurface fluids aims to understand the fluid behaviour at reservoir conditions for assessing the gas storage efficiency and designing the proper schemes of injection and withdrawal [12].

To date, a few studies have reported the γ between Hydrogen and pure water (or brine) at subsurface conditions. The reported data in experiments and simulations for water and a mixture of cushion gas such as CO_2, N_2 or CH_4 in the presence of H_2 is very limited or unavailable. Table 1 summarizes previous γ studies in the presence of H_2 with different thermo-physical conditions and percentage of cushion gas. Most previous studies from Table 1 have been focused on the binary system of Hydrogen and pure water (or brine) and performed at temperatures from 275.15 to 423 K and pressures up to 70 MPa in experiments [26–31] and in simulations ([11],[32]). However, for the H_2–CH_4–H_2O system, two experimental studies [16,33] were conducted by varying percentages of cushion gas (or CH_4) from 20 % to 80 % by Ref. [33] and at 50 % CH_4 by Ref. [16], only a simulation study [11] was performed a portion at 40 % of CH_4 in the mixture. Furthermore, for the H_2–CO_2–H_2O system, only two experiments with changing the proportion of CO_2 in the mixture from 30% to 70 % were reported [17,28], but no simulation data was reported. However, until now, no data has been available in experiments and simulations for the system of H_2–N_2–H_2O. Previous studies of the system of H_2–CH_4–H_2O and H_2–CO_2–H_2O reported that the interfacial tension of the system declined by increasing the percentage of cushion gas (CO2 or CH_4) in the mixture to compare with the binary system of pure H_2/H_2O so that it could raise a concern for H_2 diffusion through the cap rock or increasing risk for storing H_2 in depleted oil/gas reservoirs [16,33]. Therefore, studying the effects of the interfacial tension under different thermal dynamics conditions and varying the percentage of cushion gas (CO_2, N_2 and CH_4) in the mixture in the presence of H_2 at the subsurface formations is crucial for implications for UHS operations and stability.

In this work, therefore, many predictions of the interfacial tension (γ) for the systems of $H_2/CO_2/H_2O$, $H_2/CH_4/H_2O$, and $H_2/N_2/H_2O$ at different pressure, temperature, and fraction of cushion gases (CO_2, N_2 and CH_4) from 10 % to 90 % were conducted by using molecular dynamics simulation. Comparisons between the predicted γ results and experimental and simulation data from previous research were made. The achieved results deliver extending or new γ data in simulation for the systems of $H_2/CO_2/H_2O$, $H_2/CH_4/H_2O$, and $H_2/N_2/H_2O$. The findings of this study support assessing the stability and long-term practicality of several primary Underground Hydrogen Storage (UHS) in de-risking and proceeding safely and efficiently for large-scale implementation of UHS.

This research is organized into sections: Section 2 explains the simulation setup and model and the methods used for MD simulation. In Section 3, the results of simulations are found and discussed, and Section 4 provides a summary and conclusion.

Table 2
The values of parameters for Lennard Jones and Coulombic interactions.

Models	Atom	σ (nm)	ε (kJ/mol)	q (e)
H_2 (IFF)	H	0.2918	0.064	0.000
N_2 (IFF)	N	0.3670	0.279	0.000
CO_2	C	0.2757	0.234	0.651
(EPM2)	O	0.3033	0.668	−0.326
CH_4	C	0.3500	0.276	−0.240
(OPLS)	H	0.2500	0.126	0.060
H_2O (TIP4P/2005)	H	0.0000	0.000	0.524
	O	0.3159	0.775	−1.048

2. Methodology

All molecular dynamics simulations were conducted in this study using the open-source LAMMPS program [34] to predict interfacial tension at temperatures of 300 K, 323 K–343 K and pressure from 1.0 to 70 MPa. Initial configurations for simulation boxes were built with Packmol [35]. And the OVITO software [36] is used for data visualization.

2.1. Force field selection

The intermolecular potential forces employed in this study are divided into van der Waals and electrostatic interactions. The Lenard-Jones (L-J) 12–6 potential [37] was used to describe the van der Waals intermolecular potential force (nonbonded) as in equation (2).

$$U_{vdw} = 4\varepsilon_{ij}\left[\left(\frac{\sigma_{ij}}{r_{ij}}\right)^{12} - \left(\frac{\sigma_{ij}}{r_{ij}}\right)^{6}\right] \quad (2)$$

where ε_{ij} is the depth of potential well between atoms i and j at the distance between atoms r_{ij}, and σ_{ij} is the effective distance of atoms.

The Lorentz-Berthelot mixing rule [38] was applied to define the parameters of van der Waals interaction between unlike atoms, as shown in equation (3)

$$\sigma_{ij} = \left(\sigma_{ij} + \sigma_{ij}\right) \Big/ 2 \text{ and } \varepsilon_{ij} = \sqrt{\varepsilon_{ij}\varepsilon_{ij}} \quad (3)$$

Coulomb's law [39] was used to calculate electrostatic interactions according to the equation (4):

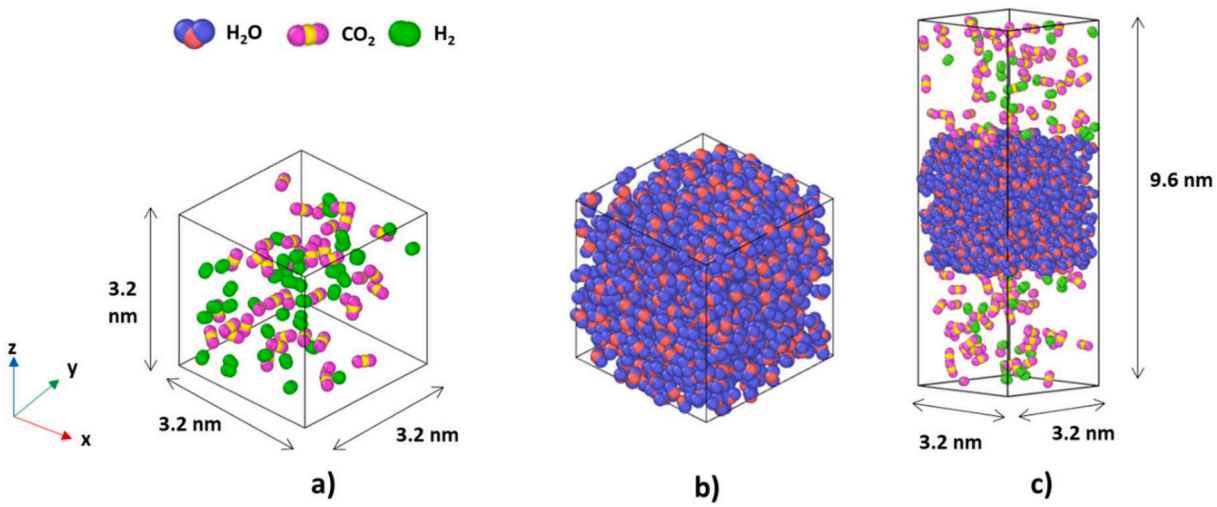

Fig. 3. A snapshot of initial arranges of H_2O, CO_2 and H_2 in simulation boxes: a) a mixed gas of CO_2 and H_2, b) bulk water, and c) a gas mixture of H_2–CO_2–H_2O system.

$$U_{coul} = \frac{q_i q_j}{4\pi\varepsilon_o r_{ij}^2} \tag{4}$$

where q_i and q_j are the partial charges on atoms *i* and j, ε_o is the vacuum permittivity.

For modelling water molecules, the force field of rigid TIP4P/2005 [40] was applied, while CO_2 is represented by the EPM2 force field [41]. Methane (or CH_4) is modelled by the OPLS force field [42]. And the Interface force field or IFF [43] was applied to both N_2 and H_2 molecules. Table 2 summarizes the L-J potential parameters and charges used for simulations in this study.

2.2. Simulation details

The simulation approach was followed from previous studies [44,45] by equilibrating simulation boxes independently prior to merging the simulation boxes, as in Fig. 3. At the beginning step, the simulation box with a size of 3.2 nm × 3.2 nm x 3.2 nm are made and to generate the initial structures and three dimensions were applied the periodic boundary conditions [46]. A number of cushion gas molecules (CO_2, N_2, or CH_4) and H_2 molecules were initialized in the simulation box based on different conditions of temperature, pressure and fraction, which vary from 8 to 515 molecules. Another simulation box was also set up by placing 1088 H_2O molecules. After the initialization of molecules in the simulation boxes, a required energy minimization was also carried out before running the simulations [44,46]. The Maxwell-Boltzmann distribution [46] was used to create the initial velocity distribution of the molecules. For the Lennard-Jones and long-range nonbonded electrostatic interactions, 10 Å was defined as the cut-off radius to ensure less than half the smallest size in the three dimensions of the simulation box. The simulation was handled with the method of Ewald [47] with a relative error of 10^{-6} for the long-range electrostatic interactions. Using the SHAKE [48,49] algorithm, the simulation was constrained to the bond length and angle of H_2O molecules. The timestep was assigned to be 0.5 fs to calculate the nonbonded interactions. The Nose-Hoover thermostat and barostat with a relaxation time of 1 ps were also applied to control temperature and pressure while running the simulation. The simulations were run initially under NVT for a 0.5 ns ensemble before switching to an NP_zT ensemble with a 5 ns to ensure the obtained density values from the simulation near the value of the experimental data's NIST database [50]. Specifically, the NP_zT ensemble was used to modify the length of the simulated box in the z-direction only, and the x-length and the y-length were kept unchanged [45,46]. In the second step for predicting interfacial tension, a rectangular simulation box merged with water in the middle and a mixture of cushions gas (CO_2 N_2 or CH_4) and H_2 gas on both sides, as displayed in Fig. 4. The system equilibrated at the desired pressure and temperature for 5.5 ns under the NVT ensemble. Data was collected at the remaining 5 ns of simulation as a production stage for interfacial tension prediction.

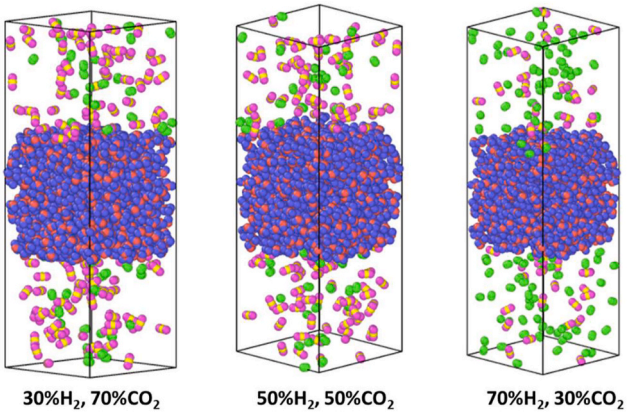

Fig. 4. An illustration of varying mole fractions of H_2 and cushion gas (CO_2).

2.3. Interfacial tension

The interfacial tension (γ) can be obtained for the H_2O and mixture of cushion gas in the presence of H_2 as in equation (5).

$$\gamma = \gamma_{sim} + \gamma_{tc} \tag{5}$$

where γ_{sim} is the interfacial tension calculated from simulation by employing Kirkwood's mechanical method [51], as described in equation (6)

$$\gamma_{sim} = \frac{L_z}{2}\left(P_{zz} - \frac{P_{xx} + P_{yy}}{2}\right) \tag{6}$$

where L_z is the length of the simulated system along the z-axis, and the three components of tensor pressure along the x-direction, y-direction and z-direction were defined as P_{xx}, P_{yy} and P_{zz}.

γ_{tc} is the tail correction applied by following the Sun's approach [52] to calculate the impacts of truncating intermolecular potentials.

Table 3
Predicted γ(H_2–CO_2–H_2O), γ(H_2–N_2–H_2O) and γ(H_2–CH_4–H_2O) at different pressure and temperature. The standard error is displayed in parentheses.

Temperature	Pressure	Interfacial tension, γ (mN/m)		
(K)	(MPa)	H_2–CO_2–H_2O	H_2–CH_4–H_2O	H_2–N_2–H_2O
300	**1**	62.9 (0.6)	64.4 (0.5)	64.0 (0.5)
	5	61.8 (1.0)	63.0 (0.5)	62.2 (0.4)
	10	59.5 (0.5)	62.6 (0.8)	62.4 (0.7)
	20	57.5 (1.0)	60.6 (0.9)	61.1 (0.9)
	30	53.1 (0.8)	60.2 (1.2)	60.5 (0.4)
	50	49.8 (1.0)	59.9 (1.1)	59.3 (0.7)
	70	45.9 (1.1)	59.4 (1.0)	59.5 (0.6)
323	**1**	59.1 (0.7)	60.5 (0.9)	60.3 (0.4)
	5	56.5 (1.0)	60.2 (0.7)	59.7 (0.5)
	10	55.6 (0.5)	59.2 (0.6)	59.9 (0.6)
	20	54.4 (1.0)	56.9 (0.8)	58.9 (1.1)
	30	52.1 (0.7)	56.6 (0.9)	58.4 (0.7)
	50	45.6 (1.0)	57.0 (0.3)	57.9 (0.5)
	70	45.8 (0.7)	57.1 (0.6)	56.5 (0.5)
343	**1**	58.6 (1.0)	56.8 (0.3)	57.3 (0.4)
	5	54.5 (0.2)	56.6 (0.3)	57.2 (0.3)
	10	53.4 (0.6)	57.0 (0.2)	56.4 (1.0)
	20	52.0 (1.1)	56.8 (0.2)	55.8 (1.0)
	30	49.8 (1.1)	54.6 (0.6)	55.5 (0.6)
	50	46.7 (0.8)	55.2 (0.5)	54.6 (1.1)
	70	42.2 (1.1)	54.2 (0.8)	55.4 (0.6)

3. Results and discussion

3.1. Interfacial tension as a function of pressure and temperature

The interfacial tension of H_2–CO_2–H_2O, H_2–N_2–H_2O, and H_2–CH_4–H_2O in different conditions of temperatures from 300 K to 343 K and pressure from 1.0 MPa to 70 MPa are reported in Table 3. The mole fracture of mixture gas was decided to select a ratio of 70:30 mol for H_2:CO_2, H_2:N_2 and H_2:CH_4, because this ratio is similar to that performed in previous experimental studies ([28], Isfehani et al., 2023). However, there is unavailable experiment data for comparing with the results of the H_2–N_2–H_2O system, so the experimental values from H_2/H_2O [11,28] and CO_2/N_2/H_2O [53,54] were used for comparison purposes.

γ(H_2–CO_2-water), as a function of pressure and temperature, is displayed in Fig. 5. Simulated outcomes indicated a similar trend to the experimental data ([28]; Isfehani et al., 2023). The γ at temperatures 300 K and 323 K are lower than the experimental data by around 12 % when the pressure is below the critical pressure of CO_2 (or less than 7.6 MPa). In contrast, the degree of agreement was improved as increasing pressure was higher at 7.6 MPa. The γ data at elevated pressure (over 50 MPa) are likely constant or altered very slightly, revealing no or minor dependence on temperature.

γ(H_2–N_2-water) was found to generally decrease with increasing pressure and temperature, as displayed in Fig. 6, demonstrating agreement with experimental values of the H_2/water [28] and the CO_2/N_2/water system [53,54]. Specifically, the simulated results are less than H_2/water caused by presenting N_2 molecules and higher than the CO_2/N_2/water due to the presence of H_2 in the system. However, at fixed temperatures (300 K, 323 K and 343 K), the reduction rate of the γ (N_2–H_2-water) is lower than the H_2–CO_2-water system, which can be explained due to the density of CO_2 being heavier than the density of N_2. Furthermore, when pressure increases above 30 MPa, the γ data tends to be unchanged or constant.

γ (H_2–CH_4-water) reported that it decreased with increasing both temperature and pressure, Fig. 7. The γ is an analogous trend in comparison to the experiment and simulation data of γ(CH_4–H_2O) and γ(H_2–H_2O). However, the γ values are lower than the system of H_2/H_2O [11,28] at a fixed temperature or pressure. The lower γ values are caused by the presence of CH_4 molecules in the mixture gas, which increases the density of CH_4 molecules at the interface. In contrast, when pressure is over 10 MPa, the simulation values of the H_2–CH_4-water system are higher than the CH_4-water system in presenting H_2 molecules in the

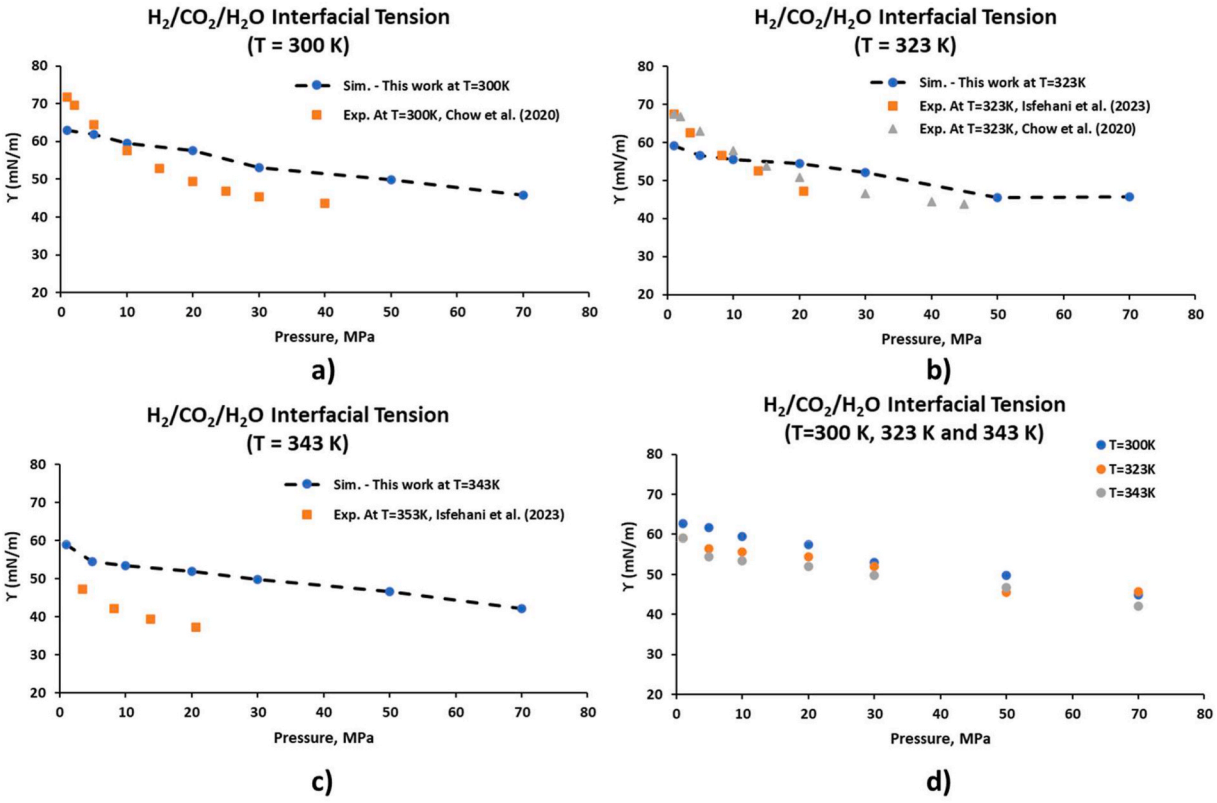

Fig. 5. Pressure dependence of γ((H_2–CO_2–H_2O): (a) at T = 300 K, (b) at T = 323 K, (c) at T = 343 K and (d) Comparison at different temperature conditions.

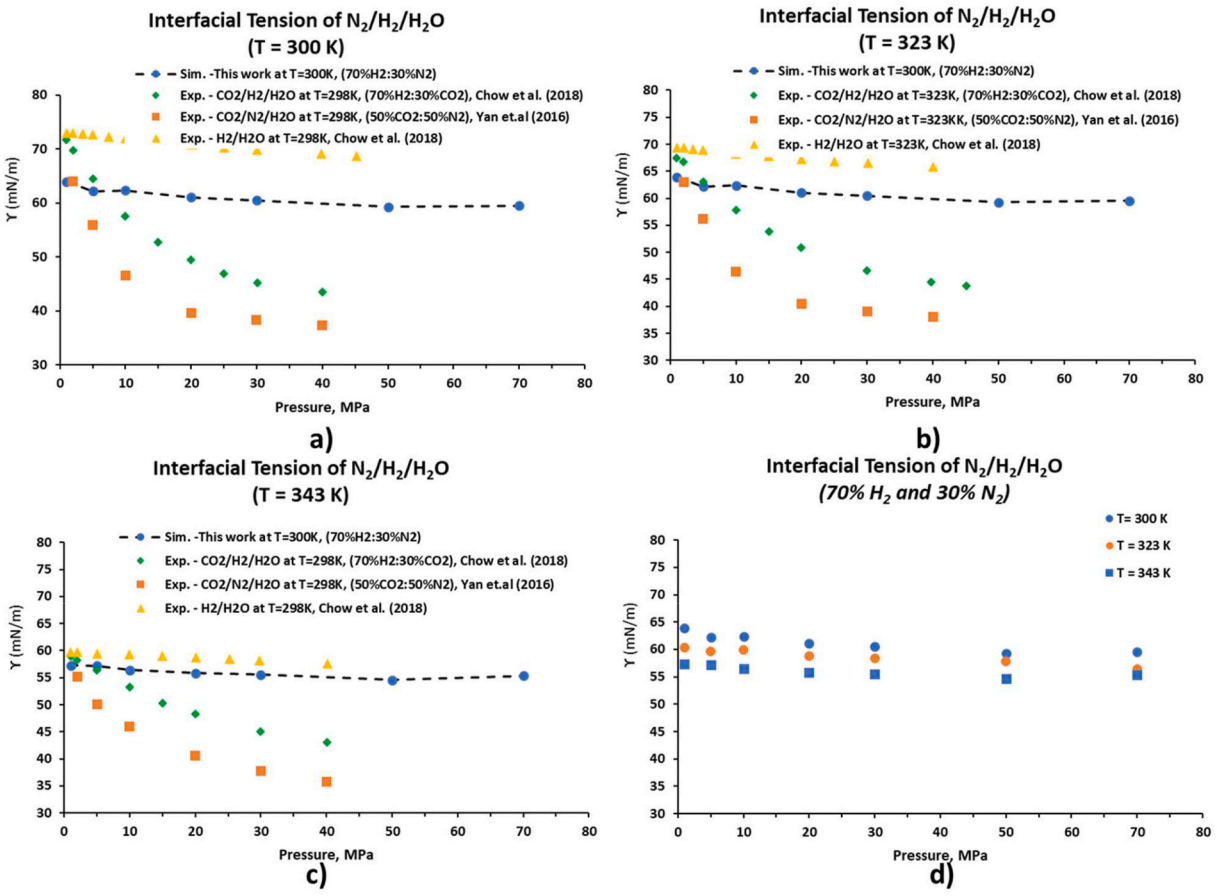

Fig. 6. Pressure dependence of γ(H_2–N_2–H_2O): (a) at T = 300K, (b) at T = 323K, (c) at T = 343K and (d) Comparison at different temperatures.

mixture gas. The cause is that the intermolecular interaction of CH_4 molecules with H_2O at the interface [55] is more substantial than H_2 with H_2O. In addition, the γ data tends to be changed slightly or unchanged when pressure increases above 30 MPa.

3.2. *Interfacial tension as a function of the fraction of cushion gases (CO_2, N_2 and CH_4)*

The interfacial tension of H_2–CO_2–H_2O, H_2–N_2–H_2O, and H_2–CH_4–H_2O in varying fractions at t conditions of 300 K and 10 MPa are reported in Table 4. The mole fraction of H_2 changed from 10 % to 90 % in the mixture gas, including CO_2 or N_2 or CH_4. While only the H_2–CO_2-water system is available experimental data [17,28] for comparison, both the H_2–N_2–H_2O and H_2–CH_4–H_2O are unavailable literature in the experiment and simulation. So, the γ experiment data of the CO_2/H_2O [56], N_2/H_20 [54], CH_4/H_2O [57] and H_2/H_2O [28] systems were used as compared data.

Fig. 8 indicates the γ of the ternary systems of H_2/CO_2/water, H_2/CH_4/water, and H_2/N_2/water increase with increasing the fraction of H_2 in the mixture gas. The simulated γ ($H_2/CO_2/H_2O$) is a similar trend in comparison with earlier reports 16,17,28. Specifically, the simulated γ ($H_2/CO_2/H_2O$) with 70 % H_2 showed excellent agreement with experimental data [28] by about 3 %. For the N_2–H_2–H_2O, the γ values are lower than the H_2/H_20 [28] and higher than the N_2/H_20 [54]. In contrast, the γ values (CH_4–H_2–H_2O) are lower than the H_2/H_2O [28] and higher than the CH_4/H_2O [57]. Furthermore, the simulated results indicated that the γ($H_2/CO_2/H_2O$) increase rate is higher than the H_2–N_2–H_2O and H_2–CH_4–H_2O systems. At the fixed fraction of H_2, the simulated values of CO_2 are the lowest to compare with the other systems. This outcome can be caused by decreasing the amount of CO_2 molecules at the interface when increasing the presence of Hydrogen in the mixture. Furthermore, the outcomes from investigating the effects of increasing the percentage of cushion gas indicated that the interfacial tension at a low concentration of H_2 in the earlier injection stage is low (especially in the case of cushion gas is CO_2), which likely causes the injected H_2 at depleted reservoirs to escape through the caprock. The findings from simulation works validated and confirmed previous experimental studies [12,16,28]. Hence, the injection scheme for UHS suggests attention to selecting a proper ratio of cushion gas and H_2 to be safe and more efficient for large-scale implementation of Underground Hydrogen Storage.

The γ of ternary systems of $H_2/CO_2/H_2O$, $H_2/CH_4/H_2O$, and $H_2/N_2/H_2O$ decrease with increasing pressure and temperatures and increase with increasing H_2% in the mixture. At constant pressure, the $H_2/N_2/H_2O$ system showed the highest γ value, while the $H_2/CO_2/H_2O$ system received the lowest γ value. This outcome is explained by increasing the quantity of molecules adsorbed (or intermolecular forces) at the interface [55]. At a fixed temperature, the γ value of $H_2/CO_2/H_2O$ needs lower pressure to reach an unchanged or plateau for comparison to the γ value of $H_2/CH_4/H_2O$ and $H_2/N_2/H_2O$ due to the number of adsorptions of CO_2 molecules increase at the surface, higher when compared with N_2 or CH_4 [55]. Hence, the simulated result recommends that N_2 offers an appropriate selection for cushion gas with higher interfacial tension than CO_2 and CH_4. This also aligns with the research by Ref. [58] to improve reservoir support and efficiency for implementing UHS.

Here, the extended and new γ ($H_2/CO_2/H_2O$, $H_2/CH_4/H_2O$, and $H_2/N_2/H_2O$) results from this work were carried out at a pressure from 1.0 MPa to 70 MPa and at different temperatures of 300 K, 323 K and 343 K and under various H_2% or cushion. The outcomes indicated the same trend in comparison with earlier experiments. However, there is a lack of data available on the systems of CO_2–H_2–H_2O and CH_4–H_2–H_2O and no data on N_2–H_2–H_2O to validate the predicted outcomes and

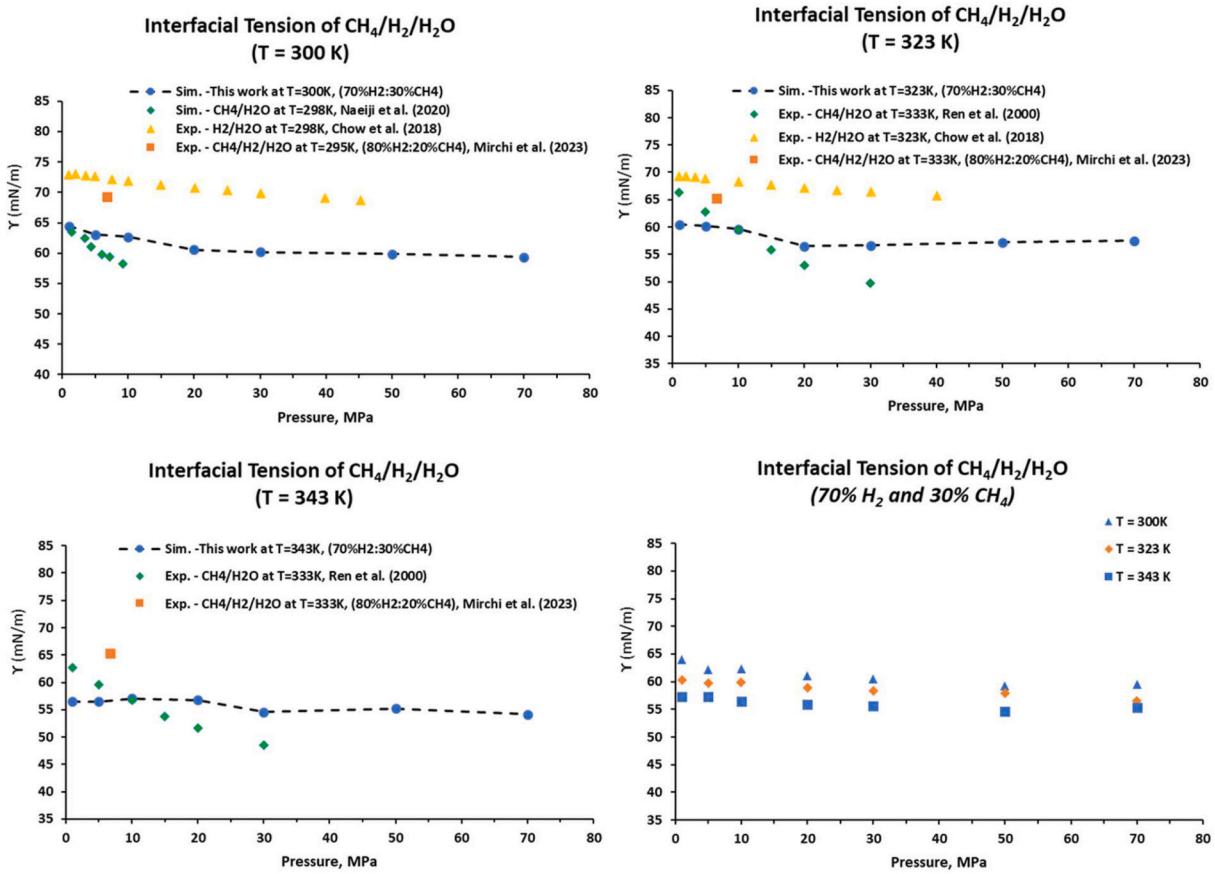

Fig. 7. Pressure dependence of γ((H_2–CH_4–H_2O): (a) at T = 300 K, (b) at T = 323 K, (c) at T = 343 K and (d) Comparison at different temperature conditions.

Table 4
Predicted γ(H_2–CO_2-water), γ(H_2–N_2-water) and γ(H_2–CH_4-water) as a function of the fraction of cushion gases (CO_2, N_2 and CH_4). The standard error is displayed in parentheses.

H_2	γ, *mN/m (P = 10 M Pa and T = 300 K)*		
Mol, %	$CO_2/H_2/H_2O$	$CH_4/H_2/H_2O$	$N_2/H_2/H_2O$
10	51.0 (0.9)	60.2 (0.3)	61.7 (0.7)
30	55.0 (1.0)	61.2 (1.1)	61.9 (0.4)
50	57.7 (0.6)	61.4 (0.8)	62.0 (0.9)
70	59.5 (0.5)	62.6 (0.8)	62.5 (0.7)
90	63.0 (0.3)	63.5 (0.7)	64.4 (1.0)

significant alterations between this work's simulation data and former experimental data. Furthermore, the difference in the γ values from simulation and experiment data can be caused by choosing forefield models [59], employing a combining rule from the Lorentz-Berthelot [60] and the size of the simulation box (Li et al., 2013). In addition, results indicated a gap difference between the predicted γ and experiment data can be caused by finite size effects when pressure is low (or a small number of H_2 molecules in the system).

4. Summary and conclusions

The interfacial tension (γ) of water and a mixture of cushion gas such as CO_2, N_2, or CH_4 in the presence of H_2 under different geo-storage conditions is vital for evaluating the storage capacity and containment security of H_2 in geo-storages. This study was conducted to fill gaps of very limited or unavailable data in experiments and simulations to investigate Hydrogen's effects when exposed to cushion gas.

1. Molecular dynamics simulations were conducted to predict interfacial tension (γ) for various ternary (CO_2–H_2–H_2O, N_2–H_2–H_2O, and CH_4–H_2–H_2O) systems at different temperatures (300 K, 323K, and 343 K) and a range of pressure from 1.0 to 70 MPa and varying concentration of cushion gas from 10 % to 90 %.
2. The γ values of CO_2–H_2–H_2O, N_2–H_2–H_2O, and CH_4–H_2–H_2O systems, as a function of pressure and temperature, decreased as increasing pressure and temperature. At fixed temperatures (300K, 323K, and 343K), the reduction rate of the γ (N_2–H_2-water and CH_4–H_2-water) is lower than the CO_2–H_2-water system. At the fixed pressure, the γ (CO_2–H_2-water system) is the lowest compared to the other systems. In addition, at high pressure (above 30 MPa), the γ data tends to be changed slightly or unchanged.
3. The γ values, as a function of H_2 fraction, increased with increasing the fraction of H_2 in the mixture gas. At the fixed fraction of H_2, the γ (N_2–H_2-water and CH_4-water) is higher than the CO_2–H_2-water system.
4. The findings noted that selecting a fraction of cushion gas (in the case of CO_2) with H_2 at the initial injection period is vital to avoid the risk of the injected H_2 escaping via the caprock. Furthermore, the cushion gas with N_2 is a reasonable selection to compare with CO_2 and CH_4 to improve reservoir support and minimize risk for implementing UHS.
5. It suggests further study on different force fields and simulation box sizes to select a proper setup or configuration (especially at low pressure) to improve the difference γ between simulation and experiment data. Furthermore, further research and development should investigate which ratio of cushion gas and the injected H_2 during the injection and withdrawal process are suitable, efficient, and safe for large-scale implementation of UHS.

This study's results deliver extending or new γ data in simulation for

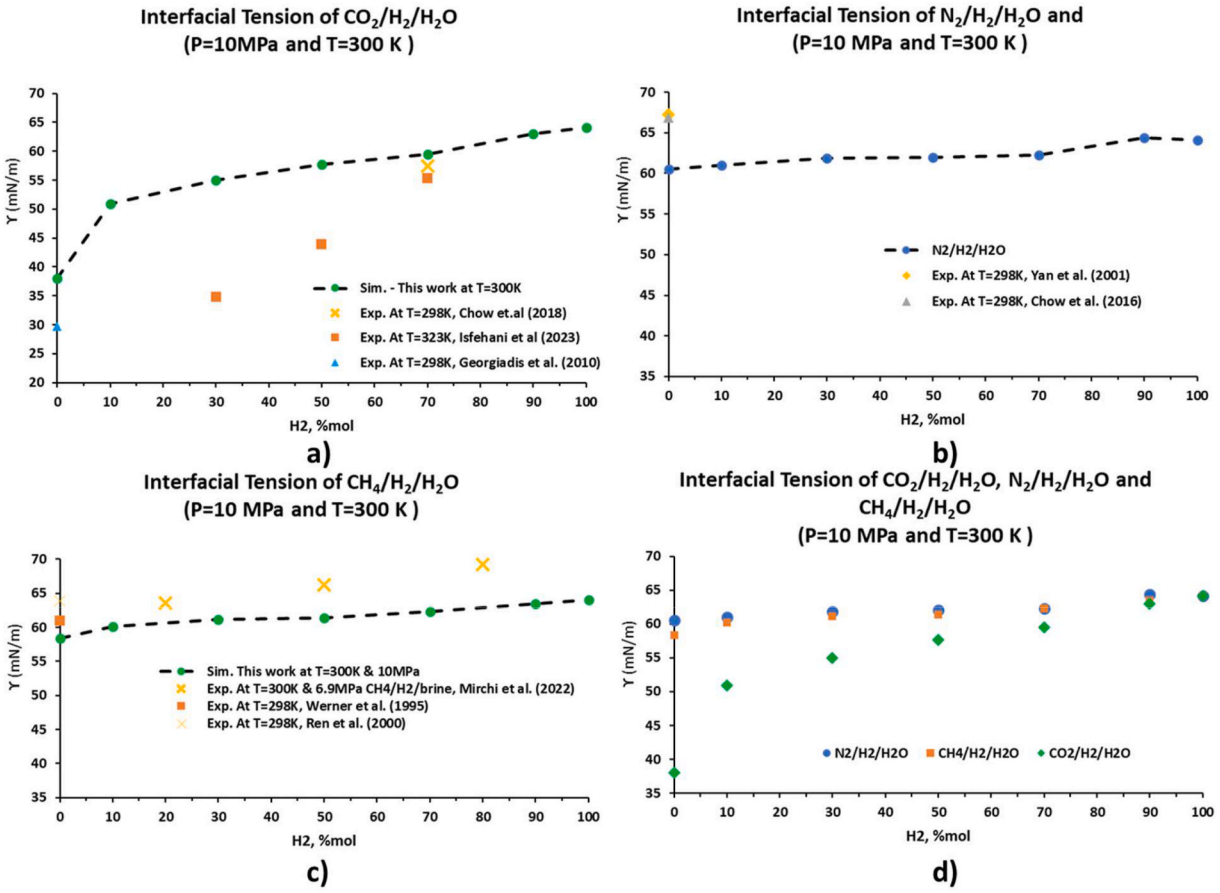

Fig. 8. γ as a function of the fraction of cushion gases (CO_2, N_2 and CH_4) at T = 300 K for (a) H_2–CO_2–H_2O system, (b) H_2–N_2–H_2O, (c) H_2–CH_4–H_2O and (d) Comparison at different temperature conditions.

the $CO_2/H_2/H_2O$, $N_2/H_2/H_2O$ and $CH_4/H_2/H_2O$ systems under different geo-storage conditions. This research contributes to understanding the flow characterization and fluid behaviour in the presence of H_2 and cushion gas at reservoir conditions for selecting and designing the proper schemes of injection and withdrawal. Furthermore, it can strongly contribute to de-risking and proceeding safely and efficiently at depleted hydrocarbon reservoirs for the large-scale implementation of Underground Hydrogen Storage.

Declaration of competing interest

The authors declare the following financial interests/personal relationships which may be considered as potential competing interests: Stefan Iglauer reports financial support was provided by Australia Research Council's Discovery Projects funding scheme (project DP220102907). Quoc Truc Doan reports financial support was provided by Bear and Brook Consulting.

Acknowledgements

The Australian Government supported this research through the Australian Research Council's Discovery Projects funding scheme (project DP220102907). This work is also supported by Bear and Brook Consulting. The authors are also thankful to the Pawsey Supercomputing Centre for supplying supercomputing time and resources.

Nomenclature

CCS	Carbon Capture and Storage
EPM2	Elementary Physical Models
LAMMPS	Large-scale Atomic/Molecular Massively Parallel Simulator
MD	Molecular Dynamics
NVT	Canonical Ensemble
NPT	Isothermal-isobaric Ensemble
NIST	National Institute of Standard and Technology
IFF	Interface Force Field
OPLS	Optimised Potentials for Liquid Simulations
OVITO	Open Visualization Tool
P	Pressure
P_c	Capillary Pressure
T	Temperature, Absolute
TIP4P/2005	Transferable Intermolecular Potential with Four Points for Water
UGS	Underground Gas Storage
UHS	Underground Hydrogen Storage

References

[1] Adoption of the Paris Agreement. Proposal by the president. In: Conference of the parties twenty-first session; 2015. Paris.
[2] CSIRO. National Hydrogen Roadmap – pathways to an economically sustainable hydrogen industry in Australia. 2018.
[3] Azzuni A, Breyer C. Energy security and energy storage technologies. 2018 Energy Proc 2018;155:237–58. ISSN 1876-6102.
[4] Blunt MJ, Pentland CH, El-Magrhaby R, Iglauer S. CO_2 sequestration in sandstones and carbonates. London, UK: Qatar Petroleum and Shell-Imperial College Grand Challenge Collaborative Programme on Clean Fossil Fuels Progress Meeting; 2011. 26th January 2011.
[5] Zivar D, Kumar S, Foroozesh J. Underground hydrogen storage: a comprehensive review. Int J Hydrogen Energy 2020;2020. https://doi.org/10.1016/j.ijhydene.2020.08.138. ISSN 0360-3199.
[6] Tarkowski R. Underground hydrogen storage: characteristics and prospects. Renew Sustain Energy Rev 2019;105:86–94.

[7] Pan B, Yin X, Ju Y, Iglauer S. Underground hydrogen storage: influencing parameters and future outlook. Adv Colloid Interface Sci 2021;294:102473.

[8] Heinemann N, Booth MG, Haszeldine RS, Wilkinson M, Scafidi J, Edlmann K. Hydrogen storage in porous geological formations onshore play opportunities in the midland valley (Scotland, UK). Int J Hydrogen Energy 2018:20861–74. 2018.

[9] Simbeck DR. CO_2 capture and storage—the essential bridge to the hydrogen economy. 2004 Energy 2004;29(9–10):1633–41. ISSN 0360-5442.

[10] Davood Z, Sunil K, Jalal F. Underfround hydrogen storage: a comprehensive review. International Journal of Hydrogen Storage 2021;46(Issue 45):23436–62. 1 July.

[11] Doan QT, Keshavarz A, Miranda RC, Behrenbruch P, Iglauer S. Molecular dynamics simulation of interfacial tension of the CO_2-CH_4-water and H_2-CH_4-water systems at the temperature of 300 K and 323 K and pressure up to 70 MPa. J Energy Storage 2023;66. https://doi.org/10.1016/j.est.2023.107470.

[12] Gbadamosi AO, Muhammed NS, Patil S, Shehri D, Al B, Haq EI, Epelle M, Mahmoud Kamal MS. Underground hydrogen storage: a critical assessment of fluid-fluid and fluid-rock interactions. J Energy Storage 2023:108473. https://doi.org/10.1016/j.est.2023.108473.

[13] Curtis MO. Carbon dioxide as cushion gas for natural gas storage. J Energy & Fuels 2003;17:240–6.

[14] Mahdi K, Behnam S, Mojtaba A. Role of cushion gas on underground hydrogen storage in depleted oil reservoirs. J Energy Storage 2022;45(2022):103783.

[15] Nasiru SM, Bashirul H, Dhafer AS. Role of methane as cushion gas for hydrogen storage in depleted gas reservoirs. Int J Hydrogen Energy 2023;48(76):29663–81. 5 September 2023.

[16] Alanazi A, Yekeen N, Ali M, Ali M, Abu-Mahfouz IS, Keshavarz A, Iglauer S, Hoteit H. Influence of organics and gas mixing on hydrogen/brine and methane/brine wettability using Jordanian oil shale rocks: implications for hydrogen geological storage. J Energy Storage 2023;62. https://10.1016/j.est.2023.106865.

[17] Isfehani Z Dalal, Sheidaie A, Hosseini M, FahimpourJ, Iglauer S, Keshavarz A. Interfacial tensions of (brine + H_2 + CO_2) systems at gas geo-storage conditions. J Mol Liq 2023;374:121279. https://doi.org/10.1016/j.molliq.2023.121279.

[18] Li Z, Dong M, Li S, Huang S. CO_2 sequestration in depleted oil and gas reservoirs—caprock characterization and storage capacity. Energy Convers Manag 2006;47(11–12):1372–82. 2006.

[19] Iglauer S, Pentlan CH, Busc A. CO_2 wettability of seal and reservoir rocks and the implications for carbon geo-sequestration. Water Resour Res 2014;51(1):729–74. https://doi.org/10.1002/2014WR015553.

[20] Iglauer S. CO_2–Water–Rock wettability: variability, influencing factors, and implications for CO_2 geostorage. Acc Chem Res 2017;50(5):1134–42. 2017.

[21] Iglauer S. Dissolution trapping of carbon dioxide in reservoir formation brine – a carbon storage mechanism. 2011. 2011.

[22] Al-Khdheeawi, Vialle S, Barifcani A, Sarmadivaleh M, Iglauer S. Impact of reservoir wettability and heterogeneity on CO_2-plume migration and trapping capacity. 2017 EA International Journal of Greenhouse Gas Control 2017;58:142–58.

[23] Iglauer S. Optimum geological storage depths for structural H_2 geo-storage S. J Petrol Sci Eng 2022;212:109498.

[24] Espinoza DN, Santamarina JC. CO_2 breakthrough-Caprock sealing efficiency and integrity for carbon geological storage. Int J Greenh Gas Control 2017;66(2017):218–29.

[25] Abramov A, Keshavarz A, Iglauer S. Wettability of quartz surfaces under carbon dioxide geo-sequestration conditions. A theoretical study 2019. https://ro.ecu.edu.au/theses/2232.

[26] Hosseini M, Fahimpour J, Ali M, Keshavarz A. H_2− brine interfacial tension as a function of salinity, temperature, and pressure; implications for hydrogen geo-storage. J Petrol Sci Eng 2022;213:110441. https://doi.org/10.1016/j.petrol.2022.110441.

[27] Massoudi R, King ADJ. Effect of pressure on the surface tension of water. Adsorption of low molecular weight gases on water at 25. J Phys Chem 1974;78(1974):2262–6.

[28] Chow YF, Maitland GC, Trusler JPM. Interfacial tensions of (H_2O + H_2) and (H_2O + CO_2 + H_2) systems at temperatures of (298–448) K and pressures up to 45 MPa. Fluid Phase Equil 2018;503(1 January 2020):112315.

[29] Kvamme B, Kuznetsova T, Hebach A, Oberhof A, Lunde E. Measurements and modelling of interfacial tension for water + carbon dioxide systems at elevated pressures. Comput Mater Sci 2007;38:506–13. 2007.

[30] Naeiji P, Woo TK, Alavi S, Ohmura R. Molecular dynamics simulations of interfacial properties of the CO_2-water and CO_2-CH_4-water systems. J Chem Phys 2020;153. https://doi.org/10.1063/5.0008114. 044701 (2020).

[31] Ren QY, Chen G, Yan W, Guo T. Interfacial tension of (CO_2 + CH_4) + water from 298 K to 373 K and pressures up to 20 MPa. J Chem Eng Data 2000;45(4):610–2. https://doi.org/10.1021/je990301s. 2000.

[32] Yang Y, Nair AK, Sun S. Molecular perspectives of interfacial properties in Water+Hydrogen system in contact with silica or kerogen. J Mol Liq 2022;385:122337. https://doi.org/10.1016/j.molliq.2023.122337.

[33] Mirchi V, Dejam M, Alvarado V. Interfacial tension and contact angle measurements for hydrogen-methane mixtures/brine/oil-wet rocks at reservoir conditions. Int J Hydrogen Energy 2022;47(82):34963–75. https://doi.org/10.1016/j.ijhydene.2022.08.056.

[34] Plimpton S. Fast Parallel algorithms for short-range molecular dynamics. J Comput Phys 1995;117:1–19. 1995.

[35] Martínez L, Andrade R, Birgin EG, Martínez JM. Packmol: a package for building initial configurations for molecular dynamics simulations. J Comput Chem 2009;30(13):2157–64. https://doi.org/10.1002/jcc.21224.

[36] Stukowski A. Visualization and analysis of atomistic simulation data with OVITO – the Open Visualization Tool. Model Simulat Mater Sci Eng 2010;18. 015012.

[37] Berendsen HJC, Grigera JR, Straatsma TP. The missing term in effective pair potentials. J Phys Chem 1987;91(24):6269–71. 1987.

[38] Frenkel D, Smit B. Understanding molecular simulation: from algoriths to application. Elsiver 2001;ume 1. 2001.

[39] Allen MP, Tildesley DJ. Computer simulation of liquids. 2017. 2nd ed. Oxford: Oxford University Press; 2017.

[40] Abascal JLF, Vega C. A general purpose model for the condensed phases of water: TIP4P/2005. 2005 J Chem Phys 2005;123:234505. https://doi.org/10.1063/1.2121687.

[41] Harris JG, Yung KH. Carbon dioxide's liquid-vapor coexistence curve and critical properties as predicted by a simple molecule model. J Phys Chem 1995;99:12021. 1995.

[42] Jorgensen WL, Maxwell DS, Tirado-Rives J. Development and testing of the OPLS all-atom force field on conformational energetics and properties of organic liquids. J Am Chem Soc 1996;118:11225. 1996.33.

[43] Wang S, Hou K, Heinz H. Accurate and compatible force field for molecular oxygen, nitrogen, and hydrogen to simulate gases, electrolytes, and hetergeneous interfaces. J Chem Theor Comput 2021;17:5198–213. 2021.

[44] Liu S, Yang X, Qin Y. Molecular dynamics simulation of wetting behavior at CO_2/water/solid interfaces. Chin Sci Bull 2010;55(21):2252–7. https://doi.org/10.1007/s11434-010-3287-0.

[45] Ofori K, Phan CM, Barifcani A, Iglauer S. An investigation of some H2S thermodynamical properties at the water interface under pressurized conditions through molecular dynamics. Mol Phys 2021. https://doi.org/10.1080/00268976.2021.2011972.

[46] Chen C, Hu W, Li W, Song Y. Model comparison of the CH_4/CO_2/water system in predicting dynamic and interfacial properties. J Chem Eng Data 2019;64(6):2464–74. https://doi.org/10.1021/acs.jced.9b00006. 2019.

[47] Ewald PP. Die Berechnung optischer und elektrostatischerGitterpotentiale. Ann Phys 1921;369:253–87. https://doi.org/10.1002/andp.19213690304.

[48] Ryckaert JP, Ciccotti G, Berendsen HJ. Numerical integration of the cartesian equations of motion of a system with constraints: molecular dynamics of n-alkanes. J Comput Phys 1977;23:327–41. https://doi.org/10.1016/0021-9991(77)90098-5.

[49] Weinbach Y, Elber R. Revisiting and parallelizing SHAKE. J Comput Phys 2005;209(1):193–206. 2005.

[50] Shen, V.K., Siderius, D.W., Krekelberg, W.P., and Hatch, H.W., Eds., NIST Standard Reference Simulation Website, NIST Standard Reference Database Number 173, National Institute of Standards and Technology, Gaithersburg MD, 20899, http://doi.org/10.18434/T4M88Q.

[51] Kirkwood JG, Buff FP. The statistical mechanical theory of surface tension. J Chem Phys 1949;17:338–43. https://doi.org/10.1063/1.1747248. 1949.

[52] Sun H. COMPASS: an ab initio force-field optimised for condensed-phase ApplicationsOverview with details on alkane and benzene compounds. Phys Chem B 1998;102(38):7338–64. 1998.

[53] Chow YF, Maitland GC, Trusler JPM. Interfacial tensions of the (CO2 + N2 + H_2O) systems at temperatures of (298–448) K and pressures up to 40 MPa. The Journal of Chenical Thermodynamics 2016;93:392–403.

[54] Yan W, Zhao GY, Chen G-J, Guo TM. Interfacial tension of (methane + nitrogen) + water and (carbon dioxide + nitrogen) + water systems. Journal of Chemical and Engineering Dada 2001;46(6):1544–8.

[55] Naeiji P, Woo TK, Alavi S, Ohmura R. Interfacial properties of hydrocarbon/water systems predicted by molecular dynamic simulations. J Chem Phys 2019;150:114703. https://doi.org/10.1063/1.5078739. 2019.

[56] Georgiadis A, Maitland G, Trusler JPM, Bismarck A. Interfacial tension measurements of the (H_2O+CO_2) system at elevated pressures and temperatures. 2010 J Chem Eng Data 2010;55:4168–75. Calculating geological storage. Energy Conversion and Management, Volume 50, Issue 2, February 2009, Pages 431.

[57] Hebach A, Oberhof A, Dahmen N, Kogel A, Edere H, Dinjus E. Tension at elevated pressures-measurements and correlations in the water + carbon dioxide system. J Chem Eng Data 2002;47:1540–6. 2002.

[58] Zamehrian M, Sedaee B. Underground hydrogen storage in a partially depleted gas condensate reservoir: influence of cushion gas. J Petrol Sci Eng 2022;212. https://10.1016/j.petrol.2022.110304.

[59] Silvestri A, Ataman E, Budi A, Stipp SL, Gale JD, Raiteri P. Wetting properties of the CO_2-water-calcite system via molecular simulation: shape and size effects. Langmuir 2019;35(50):16669–78. https://doi.org/10.1021/acs.langmuir.9b02881. 2019.

[60] Iglauer S, Ali M, Keshavarz A. Hydrogen wettability of sandstone reservoirs: implications for hydrogen geo-storage. Geophys Res Lett 2020;48. https://doi.org/10.1029/2020GL090814. e2020GL090814.